Transport Simulations for Tokamak Edge-Plasmas

T.D. Rognlien, R.H. Cohen, L.L. LoDestro, G.D. Porter, M.E. Rensink, D.D. Ryutov, and X.Q. Xu

University of California Lawrence Livermore National Laboratory,
Livermore, CA 94551, USA

e-mail contact of main author: `trognlien@llnl.gov`

Abstract. The edge plasma plays key roles in tokamak devices: it generates the edge transport-barrier yielding the L-H core confinement transition, distributes the core charged-particle energy to surrounding material surfaces, shields the core from impurities, and removes helium ash in fusion plasmas. The transport of density, momentum, and energy in the near-separatrix edge region, and the corresponding self-consistent electrostatic potential, require a two-dimensional description, here incorporated into the UEDGE code. In the direction across the B-field, both turbulent transport and classical cross-field flows are important. The role of classical flows is analyzed in detail in the presence of an assumed diffusive turbulent transport. Results and explanations are given for the generation of radial electric field near the separatrix, edge plasma asymmetries and differences between double-null DIII-D and NSTX devices, comparisons with DIII-D diagnostics, and core/edge transport coupling.

1. Introduction

Edge plasmas provide the interface between hot core plasmas and the material surfaces of the vacuum vessel in fusion energy devices. Understanding characteristics of the edge plasma is important both for predicting particle and heat fluxes onto the surfaces and for influencing the behavior of the core plasma, *e.g.*, the edge transport barrier of the H-mode confinement in tokamaks, where the edge plasma supports a high edge-temperature [1].

In recent years, substantial progress has been made in modeling two major aspects of edge plasma transport in tokamaks: classical drifts across the magnetic field, $\mathbf{B}$, (*e.g*, [2, 3, 4]) and plasma turbulence (*e.g.*, [5]). Here we focus on new developments in understanding cross-field drifts in the presence of assumed turbulent transport; a second paper at this conference focuses on advances in understanding the plasma turbulence and its effect on transport [6]. In the present paper, Sec. 2. identifies key mechanisms for radial electric field (E_r) generation, Sec. 3. compares double-null DIII-D and NSTX tokamaks, Sec. 4. compares experimental measurements for a DIII-D single-null case, and Sec. 5. discusses progress with core/edge transport coupling. Conclusions are given within each section.

2. Processes determining E_r

The radial electric field in the plasma edge is of particular interest because the shear in the poloidal $\mathbf{E}\times\mathbf{B}/B^2$ velocity is believed to play an important role in suppressing edge turbulence [1]. Previous simulations [2, 3] show that a strong negative E_r typically forms just inside the magnetic separatrix as is often observed experimentally [1]. Analysis of these type of simulations shows that the strongly negative core E_r can be understood by considering only the particle and current continuity equations with negligible sources:

$$\nabla\cdot(n\mathbf{u})\approx 0, \text{ and } \nabla\cdot\mathbf{J}=0 \tag{1}$$

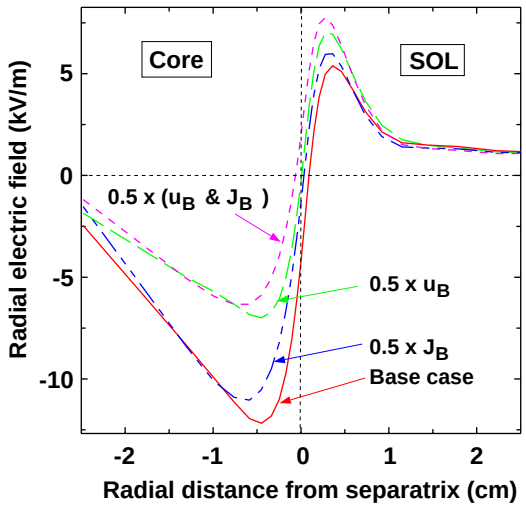

FIG. 1: Radial electric field at outer midplane for DIII-D simulation showing effects of changes to guiding-center drifts in Eq. (1).

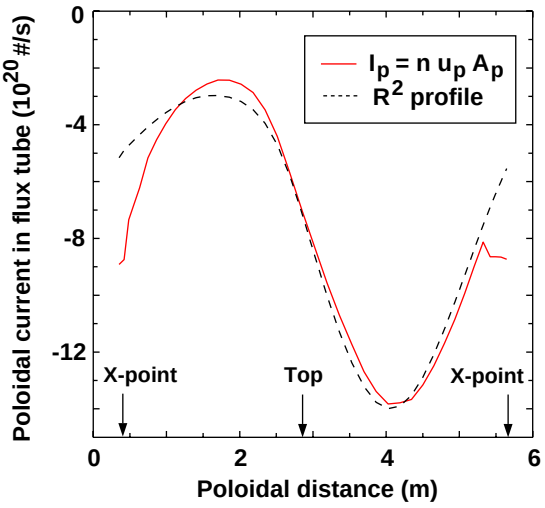

FIG. 2: Poloidal variation of ion particle current ($I_p = nu_pA_p$) just inside the separatrix from Fig. 1. R is the major radius.

where n is the plasma density, $\mathbf{u}$ is the ion velocity, and $\mathbf{J}$ is the plasma electrical current density, including $J_\parallel$ from the parallel Ohm's law and the perpendicular guiding-center $\mathbf{J}_B$. The poloidal velocity is $u_p = u_{pE} + u_{pB} + u_{p\parallel}$, here dominated by $u_{pE} = E_r/B$, with the ∇B+curvature term, u_B, and projection of $u_\parallel$ small. The radial velocity is $u_r = u_{rE}+u_{rB}+u_{ra}$, being dominated by u_{rB} in the core (u_{ra} is from anomalous diffusion). Details of the UEDGE implementation of these equations are given in Ref. [3].

Figure 1 shows the calculated E_r for the DIII-D lower-single-null tokamak configuration at 2.5 MW for four cases: a base-case, one where both $\mathbf{u}_B$ and $\mathbf{J}_B$ are reduced by a factor of 0.5, and two where $\mathbf{u}_B$ and $\mathbf{J}_B$ are separately reduced by 0.5. The ion ∇B velocity is towards the X-point. The nearly 50% reduction in $|E_r|$ is seen to be caused predominantly by the $\mathbf{u}_B$ in the ion continuity equation. The plasma density, temperatures, and $u_\parallel$ vary little among these four cases. The insensitivity of the current continuity condition to changes in $\mathbf{J}_B$ is because $J_\parallel$ can easily compensate by small changes in the nearly balancing electron pressure and $E_\parallel$ terms in parallel Ohm's law.

The change in E_r is primarily controlled by the particle continuity equation, which is analyzed by taking a small sample volume of a flux tube with sides Δr, Δx_p, and $2\pi R$. The poloidal flux variation inside the separatrix depends on the potential ϕ being nearly constant on a flux surface, giving $E_r \approx -\Delta\phi/\Delta r$, where Δr is the poloidally dependent separation of the flux surfaces. The change through the volume of $I_p \equiv nu_pA_p \approx n(\Delta\phi/B\Delta r)2\pi R\Delta r = (2\pi n/B_0R_0)\Delta\phi R^2$ must balance the change in $I_r \equiv nu_rA_r \approx nu_{rB}$, where $A_r = 2\pi R\Delta x_p$. Figure 2 confirms that $I_p \propto R^2$ inside the separatrix. The poloidal variation of ΔI_p via R^2 approximately matches that of ΔI_r via the vertical drift u_{rB}. Thus, it is convenient to apply $\Delta I_p + \Delta I_r = 0$ at the top of the machine, giving

$$E_{r,t} \approx -[0.5|u_{rB}B|(R_0/\ell_p)]_t \approx -[T_i/e\ell_p]_t \text{ leading to } E_r \approx -T_i/e\ell_p. \quad (2)$$

Here ℓ_p is the radial scale-length of ion pressure ($p_i = nT_i$) from ΔI_r, and subscript t denotes evaluation at the top of the machine. The second relation in Eq. (2) follows since ϕ and T_i are assumed constant on a flux surface. The result corresponds to $enE_r \approx \nabla_r p_i$,

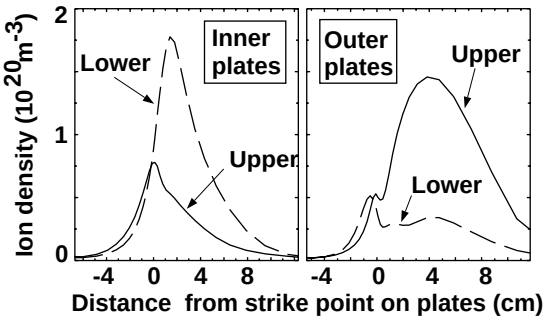

FIG. 3: Divertor plate ion density for DIII-D double-null case

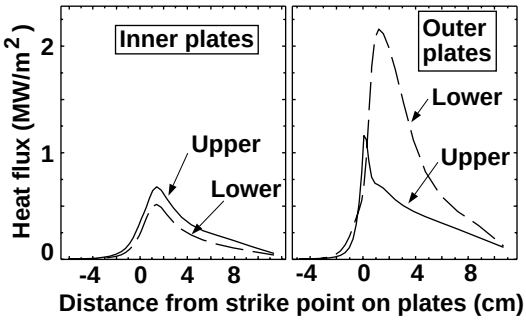

FIG. 4: Divertor plate heat flux for DIII-D double-null case

and the analysis shows why this gives an equilibrium for large u_E. Near the X-point, other terms come into the analysis. Equation (2) reproduces the core E_r in Fig. (1) to within $\sim 30\%$. Note E_r is independent of the sign of B, although ℓ_p can change. On open field lines, E_r becomes positive since there sheath and parallel electron physics give $\phi \sim T_e$, and T_e decays radially. Here we have focused on the poloidal variation of the classical $\mathbf{u}_B$ drift in steady state. It is likely that similar poloidal- and time-dependent particle fluxes can be driven by plasma turbulence [6]; if large enough, these would likewise couple through the particle continuity equation to strongly affect E_r near the separatrix.

3. Cross-field drifts for double-null DIII-D and NSTX devices

Double-null magnetic configurations can reduce the peak heat flux on divertors by splitting the power between upper and lower plates. However, even if the configuration is magnetically balanced, cross-field drifts can produce significant up/down plasma asymmetries in addition to the inboard/outboard asymmetry observed in single-null configurations.

We demonstrate the effect of the drifts with a UEDGE simulation of DIII-D in a balanced double-null configuration. The core-edge plasma density at the 92% flux surface is 3×10^{19} m^{-3} and the power into the SOL is 2.2 MW. Anomalous diffusion coefficients are 0.5 m^2/s. Plasma density and heat flux at each of the divertor plates are shown in Figs. 3 and 4, respectively. The curves refer to the standard case with ∇B downward, and interchange when the toroidal $B_t (\approx B)$ changes sign. The up/down asymmetries are due entirely to cross-field drifts. The density asymmetries in Fig. 3 can be understood as primarily from nE_r/B_t fluxes in the private-flux regions [2]; for standard B_t, these flows move particles from the lower outboard plate to the lower inner plate, and vice versa on the upper plates. For the heat flux in Fig. 4, most of the core power goes to the outer divertor plates because of increased volume there and higher outer midplane radial fluxes. The up/down asymmetry in heat fluxes on the outer plates is opposite to that for the densities in Fig. 3. The heat-flux asymmetry is primarily caused by the thermoelectric current driven by the higher T_e at the lower plate compared to the upper plate. This electron current convects electron thermal energy from the upper plate to the lower plate (0.2 MW in this case), yielding the heat flux asymmetry seen in Fig. 4. Next, to assess the relative effect of cross-drifts in conventional versus spherical tokamaks, the double-null DIII-D simulation just presented is compared to a corresponding one for NSTX. Parameters are the same, except that the power into the SOL is $P = 1.2$ MW to give the same average radial heat flux at the core boundary as used for DIII-D (40 kW/m^2). These devices have

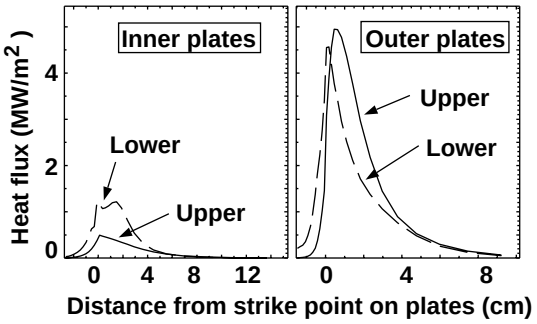

FIG. 5: Divertor plate heat flux for NSTX double-null case

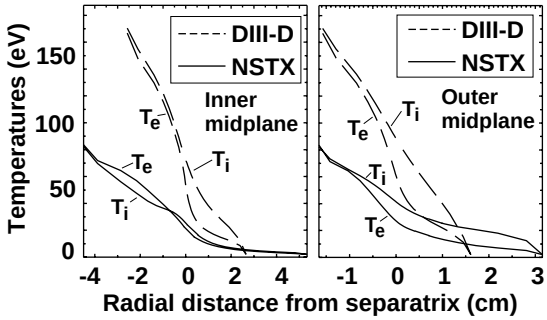

FIG. 6: Inner and outer midplane T_e and T_i profiles comparing DIII-D and NSTX cases.

similar poloidal cross-sections, but the major radius is $R = 1.7$ m in DIII-D versus 0.8 m in NSTX. The corresponding P/R values are 1.2 and 1.5 MW/m, but since these machines have different pitch of the magnetic field, P/R scaling is not expected between them. Also, $B_t = 2.0$ T in DIII-D and only $B_t = 0.3$ T in NSTX. Figure 5 shows the heat flux on the outer plates corresponding to Fig. 4; inner plate heat fluxes are much lower. Note that for NSTX, the profiles are much more up/down symmetric. The greater symmetry arises because the parallel electron current flow for NSTX is much smaller owing to the lower SOL T_e. Midplane $T_{e,i}$ profiles for NSTX and DIII-D are shown in Fig. 6. Although the radial heat flux is the same, the shorter parallel connection length for NSTX gives lower $T_{e,i}$ because of more rapid parallel heat conduction to the plates.

4. Experiment/simulation comparison for DIII-D single null

We have examined the effect of drifts in the edge and scrape-off layer plasmas of DIII-D by simulating a specific lower single-null, ohmic-heated discharge with the outer strike-point positioned on the bias ring to enable simulation of the effect of biasing as well as the effect of drifts on unbiased plasmas. Simulation of biased plasmas is ongoing. We use a fixed-fraction impurity model to give the effect of radiation cooling of the divertor plasma. Good agreement is obtained with measured upstream and downstream profiles of density and temperature with anomalous diffusivities of $D = 0.35$ m^2/s, and $\chi_{e,i} = 1.8$ m^2/s; midplane density is shown in Fig. 7. The diffusivities needed are consistent with those used in earlier simulations without drift effects [7]. The divertor region density is measured with both a divertor Thomson system and an insertable probe. Both measurements are taken along a vertical line at line R=1.48 m which passes just on the high-field side of the X-point as shown in Fig. 8. The inner leg is detached on this discharge with $T_e \approx 1$ eV. On the outer leg, the peak $T_e \approx 30$ eV. The divertor densities are quite low, as is the upstream density. The cross-field drifts seem to have a small effect on the measurable plasma parameters for this case, decreasing the density near the inner strike-point by $\sim 25\%$. The drifts do affect the poloidal flows, which should alter impurity accumulation when multispecies impurities are used.

5. Core-edge coupling

CORSICA 2, introduced in Ref. [8], self-consistently evolves whole-cross-section tokamak transport equations. The plasma core is time-advanced using the fully implicit 1D

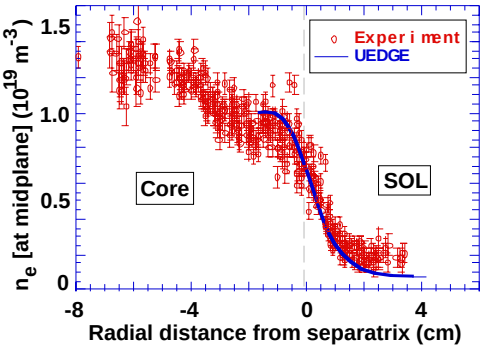

FIG. 7: DIII-D experiment/simulation comparison of midplane density profiles.

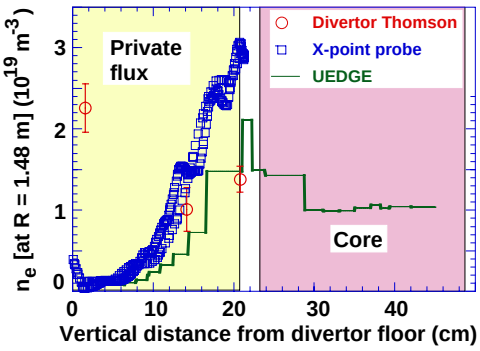

FIG. 8: DIII-D experiment/simulation comparison of divertor region density profiles.

Grad-Hogan code CORSICA 1, and the edge and SOL are simulated with a choice of edge models, the most comprehensive of which is UEDGE. Within each time-step, the core and edges codes are run sequentially and the shared boundary conditions are iterated via a Newton scheme until self-consistency is reached. The coupled fields include n_D, T_e, T_i, n_{gas}, and the angular momentum L_z. A recent focus has been on improving consistency in the core/edge transport equations for L_z. We have also improved the coupling algorithm: The coupling surface is at the innermost core surface for UEDGE (*i.e.*, it is where UEDGE's boundary condition is applied), but the core transport grid can extend over its full usual domain (*i.e.*, to a surface very near the separatrix). The core-code boundary condition is then varied internally to achieve the value requested by the Newton solver at the coupling surface. This permits improved solutions for those fields which evolve under transport, but are either not evolved by UEDGE (*e.g.*, q), or are not included among those coupled for a given simulation. It also provides a numerical test of uniform 1D overlap at the coupling surface; tests show good overlap of the two solutions.

Acknowledgments: Work performed under the auspices of the U.S. Department of Energy by the University of California Lawrence Livermore National Laboratory under contract No. W-7405-Eng-48.

References

[1] BURRELL, K.H., Phys. Plasmas **4** (1997) 1499.

[2] ROGNLIEN, T.D., *et al.*, J. Nucl. Mater. **266-269** (1999) 654.

[3] ROGNLIEN, T.D., *et al.*, Phys. Plasmas **6** (1999) 1851.

[4] CHANKIN, A.V., *et al.*, Contrib. Plasma Phys. **40** (2000) 288; GERHAUSER, H., *et al.*, *ibid*, p. 309; SCHNEIDER, R., *et al.*, *ibid*, p. 328.

[5] XU, X.Q., *et al.*, Phys. Plasmas **7** (2000) 1951.

[6] XU, X.Q., *et al.*, paper at this conference.

[7] PORTER, G.D., *et al.*, Phys. Plasmas **7** (2000) 3663.

[8] TARDITI, A., *et al.*, Contrib. Plasma Phys. **36** (1996) 132.